Digest Journal of Nanomaterials and Biostructures Vol. 18, No. 2, April - June 2023, p. 713 - 726

The effect of tungsten ions on the structural, elastic moduli, and shielding characteristics of arsenic lead phosphate glasses

B. Basha[a], Kh. S. Shaaban[b], E.A. Abdel Wahab [c,*]
[a]*Department of Physics, College of Sciences, Princess Nourah bint Abdulrahman University (PNU), P.O. Box 84428, Riyadh 11671, Saudi Arabia.*
[b]*Department of Chemistry, Faculty of Science, Al-Azhar University, P.O. 71452, Assiut, Egypt.*
[c]*Department of Physics, Faculty of Science, Al-Azhar University, P.O. Box 71524 Assiut, Egypt.*

A series of phosphate glass with the following formulation was manufactured using the melt quenching procedure: $3As_2O_3 - 37PbO - (60 - x)\ P_2O_5$- $x\ WO_3$, x = ($0 \le x \le 5$ mol. %). The glasses' physical and other structural characteristics were examined in depth. The basic structural properties of the materials were examined using a variety of characterization procedures, such as XRD and FT-IR. With increasing WO_3 concentration, the phosphate network evolves, leading to depolymerization of the glass network, according to the FT-IR analysis. With increasing WO_3, the physical, mechanical, and structural parameters were enhanced like glass density, longitudinal and shear speeds, and all elastic moduli. Because of P–O–W bonds in the glass network are stronger than P–O–P bonds, the radiation characteristics were enhanced as the content of WO_3 increased. The interpretation of the parameters showed that the glass in the statement is an excellent candidate for photon shielding applications.

(Received January 23, 2023; Accepted May 31, 2023)

Keywords: Phosphate, WO_3, FT-IR, Elastic moduli, Gamma shielding

1. Introduction

Oxide glasses that are produced from transition metal ions are attracting great scientist effort because of their pioneer applications in mechanical, thermal, and radiation. Because of their good semiconducting properties and high thermal stabilities, tungsten-based glasses among oxide glasses are attracting even more attention [1-4]. These glasses also have a low tendency to crystallize and have lower melting points than other glasses. The electron hopping phenomenon of tungsten ions between W^{4+} and W^{5+} states give these glasses their semiconducting properties [1-4]. Furthermore, introducing P_2O_5 to the structure may result in transmittance and a high increase in mechanical and radiation characteristics [5-11]. The most common materials are phosphate-based glasses, which improve the mechanical, optical, and radiation characteristics. Phosphate glasses could be used in biology, batteries, and laser technology, among other things. Other advantages of phosphate-containing glasses include high UV transmittances, low melting and glass transition temperatures, and high thermal stabilities.

P_2O_5 is a significant glass-forming oxide, and it was used to achieve the desired physical and chemical characteristics in a variety of glass systems. As_2O_3 is also a network former, with AsO_3 glasses [12-14]. The majority of the research on As_2O_3 glasses focuses on deciphering their structure using XRD and FT-IR spectra, and other techniques.

The objective of this research is to use FT-IR, mechanical, and radiation to explore the structural changes in $3As_2O_3 - 37PbO - (60 - x)\ P_2O_5$- $x\ WO_3$, x = ($0 \le x \le 5$ mol. %) glasses.

* Corresponding author: essam.ah77@gmail.com
https://doi.org/10.15251/DJNB.2023.182.713

2. Material and methods

The $3As_2O_3 - 37PbO - (60 - x)\ P_2O_5$- $x\ WO_3$, x = ($0 \le x \le 5$ mol. %) glasses in Table 1 were fabricated by mixing constituents of reagent grade purity such as PbO, $(NH_4)_2HPO_4$, As_2O_3 and WO_3. An electrical furnace used to melt the mixtures in crucibles of ceramic for 30 minutes at 1100°C. $PbO + As_2O_3 + WO_3 + 2(NH_4)_2HPO_4 \xrightarrow{\Delta} {}_{-(4NH_3+3H_2O)} \longrightarrow (PbO + WO_3 + As_2O_3 + P_2O_5) \xrightarrow{\Delta\ 1100\ ^\circ C} glasses \xrightarrow{annealing\ at\ 375\ ^\circ C} glass\ samples.$ By pouring the melts onto stainless steel plates. The manufactured samples were annealed at 375°C then cooled gradually to relieve thermal stress.

Table 1. Prepared glasses (mol, %).

code	P_2O_5	As_2O_3	PbO	WO_3
G 1	60	3	37	0 1 2 3
G 2	59	3	37	
G 3	58	3	37	
G 4	57	3	37	
G 5	55	3	37	5

The pattern of XRD obtained and the characteristic indicates that the samples in amorphous status in compositional range, as determined by X-ray diffraction. FT-IR absorption spectra in the range 400–4000 cm^{-1} were obtained using Perkin Elmer spectrometer. The KBr pellet technique was used to measure the IR absorption. The origin software program was used to deconvolute the bands and establish a baseline for the obtained data.

The glass density of synthesis glass was calculated by using the following connection: $\rho = \rho_o(\frac{wa}{wa-wl})$, and C_7H_8 as an immersion liquid. The relationship can be used to calculate the molar volume of a glass:$V_m = \frac{M}{\rho}$, M is molecular weight of the composition. Ultrasonic speeds were determined using (Echograph model 1085) and the measurements were repeated more than three times. Elastic moduli can be calculated with longitudinal waves $L = \rho v_l^2$, transverse waves $G = \rho v_t^2$, young's modulus $Y = (1 + \sigma)2G$, and bulk modulus $= L - \left(\frac{4}{3}\right)G$. The packing density V_i and dissociation energy G_i concepts were applied to compute the elastic moduli of the glasses [15-18]. $Vi = \left(\frac{3\pi}{4}\right)N_A\ (m\mathrm{R}_\mathrm{A}^3 + n\ \mathrm{R}_\mathrm{O}^3)\ m^3.mol^{-1}$, and $Gi = (\frac{1}{V_m})\sum_i GiXi$, $L = K + \left(\frac{4}{3}\right)G$, $G = 30 * (\frac{V_i^2 G_i}{V_i})$, $Y = 8.36 V_i\, G_i$, and $K = 10 V_i^2 G_i$. Poisson's ratio $\sigma = \frac{1}{2} - \left(\frac{1}{7.2 * Vi}\right)$. Acoustic impedance; $Z = v_L \rho$. Hardness; $\mathrm{H} = \frac{(1-2\sigma)\mathrm{Y}}{6(1+\sigma)}$. Debye's temperature: $\theta_D = \frac{h}{k}\left(\frac{9N_A}{4\pi\, V_m}\right)^{\frac{1}{3}} M_s$. Averages of velocity $M_s = \frac{1}{3}\left(\frac{\frac{2}{v_T^3}}{\frac{1}{v_l^3}}\right)^{\frac{1}{3}}$. The conductivity of fractal bonds $d = (G/K) * 4$. Thermal Coefficient $\alpha_{P\ =23.2\ (v_L - 0.57457)}$. Oxygen packing density and molar volume of oxygen $V_o = \left(\frac{M}{\rho}\right)\ \left(\frac{1}{\sum xini}\right)$, and $OPD = \left(\frac{1000\ C}{Vm}\right)\left(\frac{Mol}{L}\right)$. Sakar et al. [19] developed Phy-X / PSD, software to compute multiple shielding factors at wide energy range from (0.015 to 15 MeV). As Lambert law $\mu = -\frac{ln\frac{I}{I_o}}{x}$, I_0 and I represent the intensities before and after sample respectively, which represent the linear attenuation coefficient (LAC) (cm^{-1}). The mass attenuation

coefficient (MAC) was determined to be as follows: $\left(\frac{\mu}{\rho}\right) = \sum_i w_i \left(\frac{\mu}{\rho}\right)_i$. The mean free path (MFP) was calculated to be: $MEP = \left(\frac{1}{\mu}\right)$, The tenth (TVL) and half-value layer (HVL) are calculated as follows: TVL $= \left(\frac{\ln 10}{\mu}\right)$, HVL $= \left(\frac{\ln 2}{\mu}\right)$.

3. Results and discussion

3.1. Physical descriptions

As shown in Fig. 1, the XRD patterns revealed that the samples were highly amorphous. Fig. 2 shows glass system's density ρ and molar volume V_m. Density increased from 5.12 g/cm^3 to 5.58 g/cm^3. The ρ & V_m values showed an inverse relationship. The values of V_m ranged from 33.905 to 31.92 cm^3/mol. The density and weights of the replacement oxide are closely related to changes in ρ [20-25]. Meanwhile, variations in V_m could be attributed to variations in interatomic spacing within the glass structure. The heavier atomic weight and density of WO_3 (231.838 g/mol, 7.2 g/cm^3) as compared to P_2O_5 (141.945 g/mol, 2.3 g/cm^3) can be linked to the increase in density value for the fabricated glasses [26-28]. Fig. 3 depicts the variations in V_o and OPD. V_o values are decreasing, while OPD has expanded. These results can be attributed to a decrease in V_m.

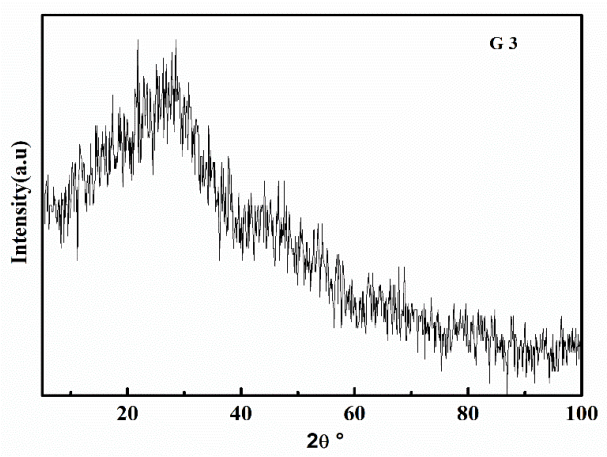

Fig. 1. XRD of synthesized samples.

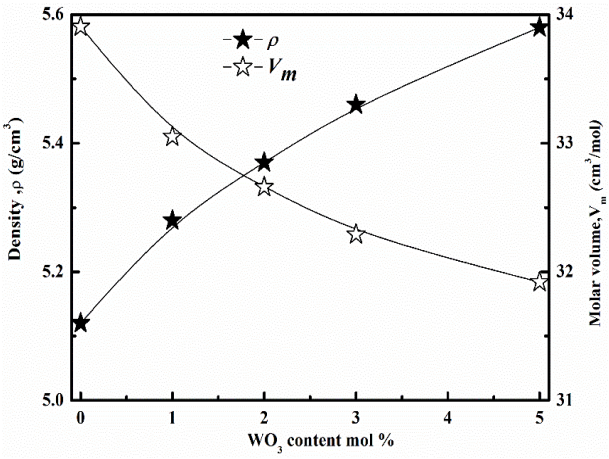

Fig. 2. ρ & V_m of prepared glasses.

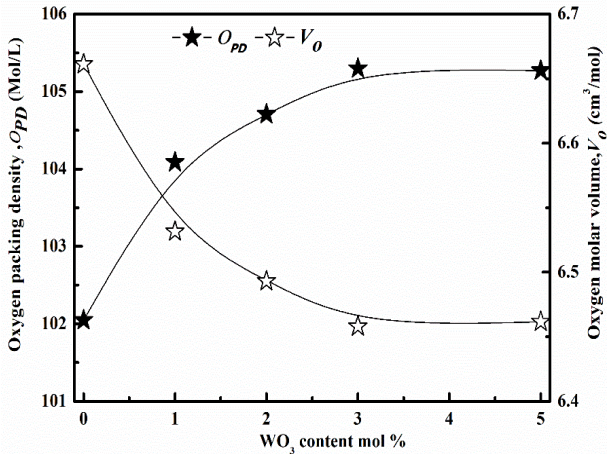

Fig. 3. V_o & OPD of prepared glasses.

3.2. Structural investigations using FT-IR

Figure 4 shows the samples' combined FT-IR spectra. Because FTIR spectra contain many asymmetric peaks, a deconvolution process was used to determine the suppressed peaks, and an example of FTIR sample deconvolution is shown in Fig. 5. Table 2 includes peak locations as well as band definitions for glasses. The bending vibration caused by the WO_5& Bending vibration (O–P–O) was represented by a band in the range of 471–492 cm^{-1} [5-11]. Bands in the 505–564 cm^{-1}, W–O bond PO_4 harmonics of P–O bending vibration & Symmetric bending vibrations of As–O [12-14]. Bands in the 673–682 cm^{-1} due to As–O bonds. Bands in the 707–753 cm^{-1}, due to P–O–P linkage has symmetric stretching modes. Bands in the 860–897 cm^{-1}, due to W–O in (W–O–As) symmetric stretching. Bands in the 900–985 cm^{-1}, owing to irregular stretching modes of the P–O–P linkages and WO_5 stretching vibrations. Bands in the 1037–1083 cm^{-1}, due to As–O bond stretching vibrations. Bands in the ~1120 cm^{-1}, due to Stretching PO_3 in an asymmetric manner. Bands in the 1225–1400 cm^{-1}, due to stretching mode of P = O. We can see an intensification in the strength of bands when W^{+5} ions are added. The depolymerization of the structure and an increase in the order degree of the studied glasses cause the broadening of some bands as the WO_3 content increases [1-4].

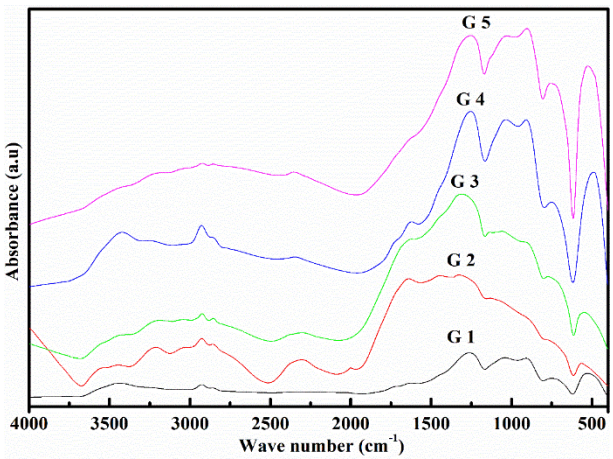

Fig. 4. FT-IR spectra as a collective.

Table 2. Locations of the peaks and band definitions.

Peak Locations (cm^{-1})					Definition
G 1	G 2	G 3	G 4	G 5	
-	-	471	487	492	Bending due to WO_5 unit & Bending vibration (O–P–O)
505	532	559	543	564	W–O bond PO_4 harmonics of P–O bending vibration & Symmetric bending vibrations of As–O
673	-	-	-	682	As–O bonds
733	714	707	730	753	The P–O–P linkage has symmetric stretching modes.
897	890	-	885	861	W–O in (W–O–As) Symmetric Stretching
-	-	901	985	955	Asymmetric stretching modes of the P–O–P linkages and WO_5 stretching vibrations
1037	1074	1053	1083	1064	As–O bond stretching vibrations
1119	-	1120	-	-	Stretching PO_3 in an asymmetric manner
1246	1269	1225	1239	1281	Stretching mode of P = O
1372	1408	1360	1307	-	

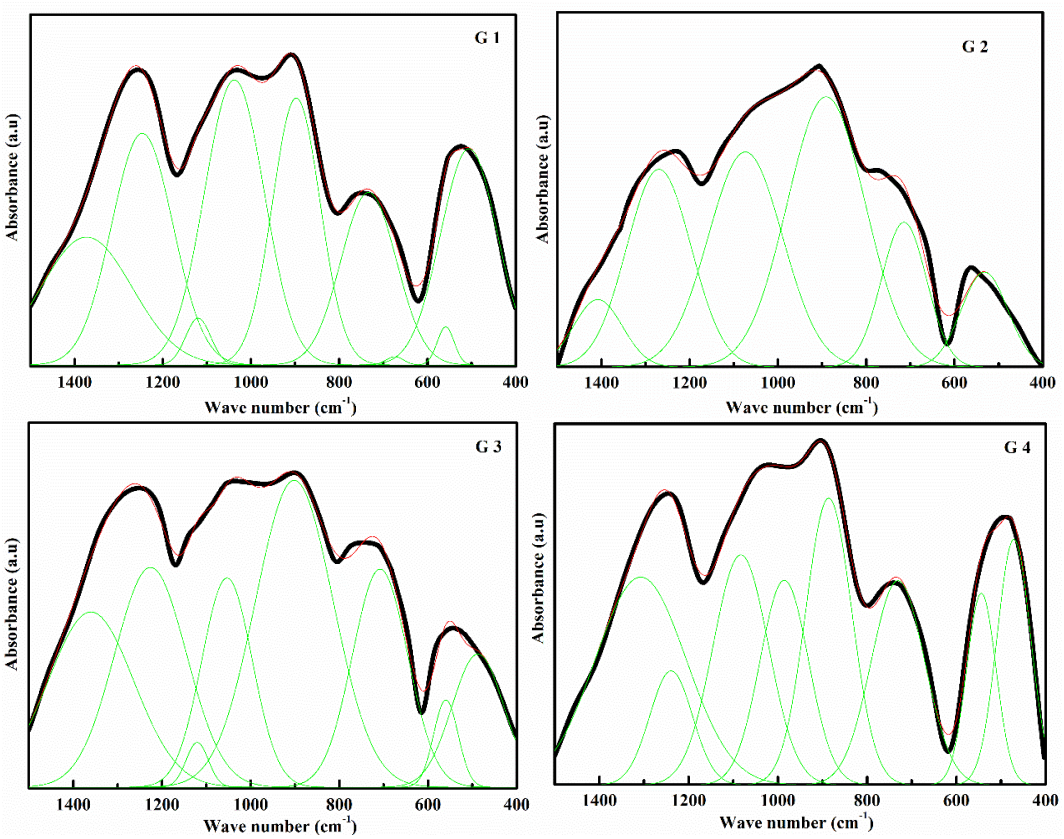

Fig. 5. FT-IR deconvolution spectra.

3.3. Ultrasonic investigations

Figure 6 depicts the velocity (v_l& v_t) of prepared glasses containing various amounts of WO_3. Table 3 shows that with an increase in WO_3 both (v_l& v_t) increments and (v_l) values greater than (v_t) [29 − 36]. v_l increases from 4530 m/s to 4745 m/s & v_t increases from 2155 m/s to 2310 m/s. The increase in (v_l& v_t) values is due to the modification of the phosphate host glass due to the presence of (W^{+5}) in the interstitial space, which also results in the exchange of P-O-P bonds to P-O-W connections. The (v_l& v_t) increases as a result, while the V_m decreases. Furthermore, increasing the WO_3 content in the host phosphate glass increases the rigidity of the glass structure, resulting in a higher (v_l& v_t).

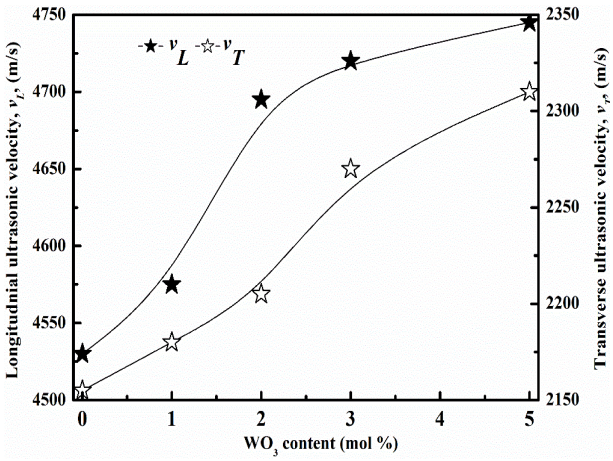

Fig. 6. (v_l& v_t) of prepared glasses.

The elastic moduli with various amounts of WO_3 are presented in Fig. 7. The elastic moduli appeared to increment with an increment in WO_3, according to the graph. L increase from 105 GPa to 125 GPa, G increase from ~23 GPa to ~30 GPa, K increase from ~73 GPa to ~86 GPa, & Y increase from ~64 GPa to ~80 GPa. Table 3 contains the detailed elastic moduli values. The glass becomes stiffer when WO_3 is exchanged into the phosphate glasses, and the density and elastic moduli both increases.

The H, d, Z& σ of the glass system are shown in Fig. 8. H increase from 2.32 GPa to 3.08 GPa. The observed increase in H, Z value is related to an increment in the stiffness of the glass construction. The M_s& θ_D of the glass, the system is exposed in Fig. 9. T_s& αp of the glass system is exposed in Fig. 10. These parameters increased as WO_3 content increased according to the above observations.

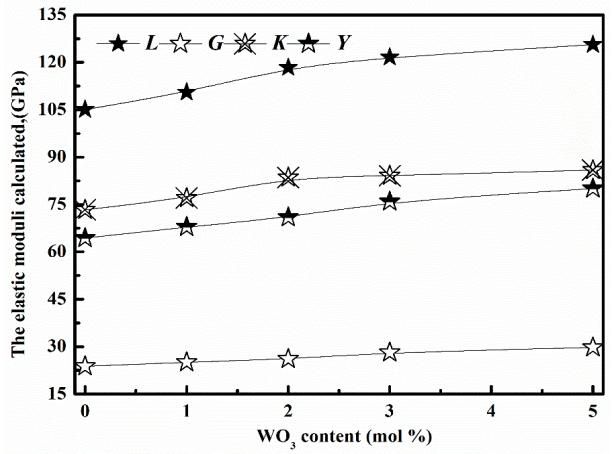

Fig. 7. (L, G, K& Y) of prepared glasses.

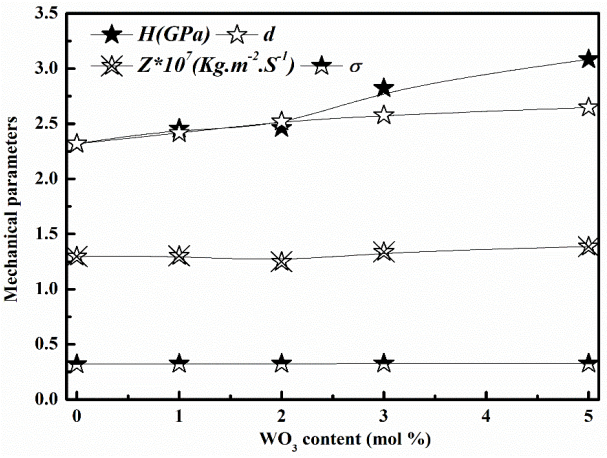

Fig. 8. ($H, d, Z\& \sigma$) of prepared glasses.

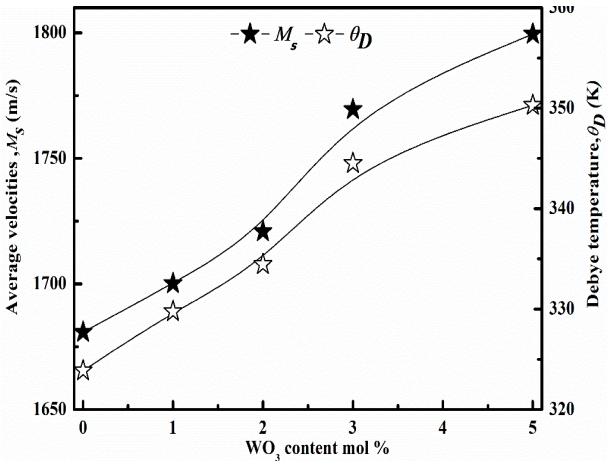

Fig. 9. ($M_s\& \theta_D$) of prepared glasses.

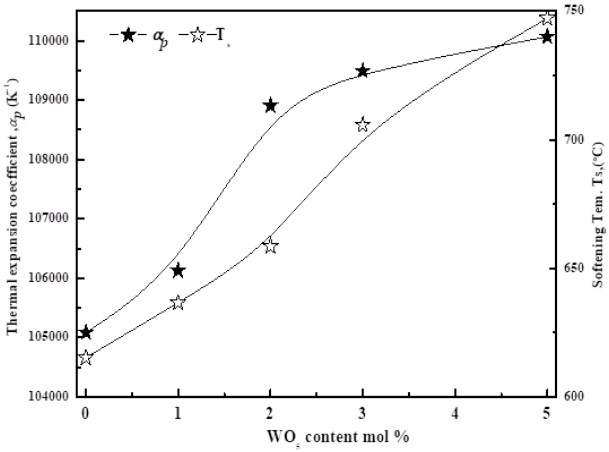

Fig. 10. ($T_s\& \alpha p$) of prepared glasses.

3.3.1. Calculation by Makishima and Mackenzie

According to Makishima-theoretical Mackenzie's calculation, [37-38] the G_i and V_i in glasses control the values of elastic moduli. G_i and V_i values are displayed in Fig. 11. V_i increase from 0.775 to 0.802 cm^3 /mol, G_i decreases from 11.68 to 11.62 kJ/cm^3. The elastic moduli of the glass system as this calculation with various amounts of WO_3 are shown in Fig. 12. The elastic moduli appeared to increment with an increment in WO_3 content, according to the graph. L increase from 110 GPa to 116 GPa, G increase from ~30 GPa to ~31 GPa, K increase from ~70 GPa to ~74 GPa, & Y increase from ~75 GPa to ~78 GPa. Table 3 contains the detailed elastic moduli values. As explored from the obtained results of elastic moduli there is acceptable agreement between Makishima-Mackenzie model and those determined by experimental procedures.

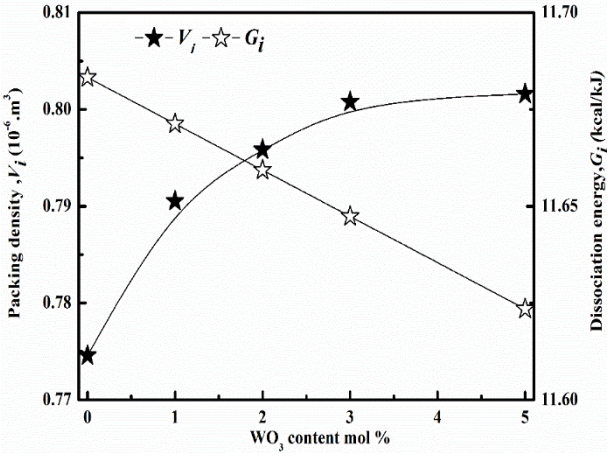

Fig. 11. (G_i & V_i) of prepared glasses.

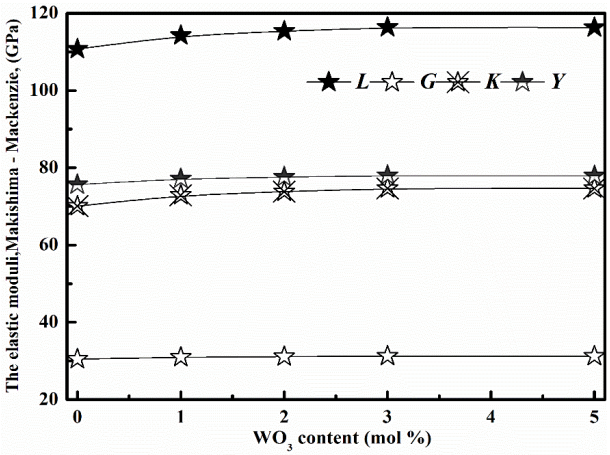

Fig. 12. ($L, G, K \& Y$) of prepared glasses as calculation by Makishima and Mackenzie.

Table 3. Values of mechanical characteristics.

Samples	G 1	G 2	G 3	G 4	G 5
V_L	4530	4575	4695	4720	4745
V_T	2155	2180	2205	2270	2310
L	105.07	110.51	118.37	121.64	125.63
G	23.78	25.09	26.11	28.13	29.78
K	73.36	77.06	83.56	84.13	85.93
Y	64.38	67.91	70.94	75.94	80.08
L_{th}	110.73	114.24	115.345	116.37	116.32
G_{th}	30.47	30.98	31.125	31.26	31.2
K_{th}	70.1	72.94	73.845	74.69	74.69
Y_{th}	75.65	77.13	77.57	77.97	77.89
V_i	0.77	0.79	0.796	0.80	0.80
G_i	11.68	11.67	11.66	11.65	11.62
V_o	6.7	6.5	6.5	6.5	6.5
O_{PD}	102.0	104.1	104.7	105.3	105.3
d	1.3	1.3	1.2	1.3	1.4
T_s	615.2	636.6	658.5	705.7	747.2
α_p	105082.7	106126.7	108910.7	109490.7	110070.7
H	2.3	2.5	2.5	2.8	3.1
M_s	1681	1700	1721	1769	1799
θ_D	324	330	334	344	350
Z	2.3	2.4	2.52	2.58	2.65

3.4. Investigations of gamma attenuation

MAC & LAC, MFP, HVL, and TVL were calculated to explore the performance arsenic lead phosphate glass doped tungsten ions like a shield material. The shielding characteristics of each glass were discovered to be dependent on the chemical composition and the energy of the incident gamma-rays. The investigation take place on wide energy range from 0.015 to15 MeV, Fig. 13 depicts adjustments in MAC values of glass samples. Fig. 13 displays that the MAC values increment as WO_3 in glass samples rises. The photon energy in the glass system also affects the MAC values. The MAC values of the glass samples rapidly decline with increasing photon energy at energy is smaller than 1 MeV. Ref.[39 –50] shows studies where similar situations have been observed. This reduction is due to the photoelectric effect, which occurs when atoms in glasses interact with gamma radiation. Energy values are inversely proportional to Compton scattering cross-section (CSP) values. As a result, in the range of $1< E < 8$ MeV, this process dominates. MAC values become almost constant after a while in the energy range greater than 8 MeV. This attitude proves the formation of the pair production process (PPP) is dominant in this energy range. In previous studies, this behavior was also observed [39 –50]. Fig. 14 depicts adjustments in LAC values of glass samples. Fig. 14 shows that the LAC values increment as WO_3 in glass samples rises. The LAC values were found to be in the same direction as the MAC values.

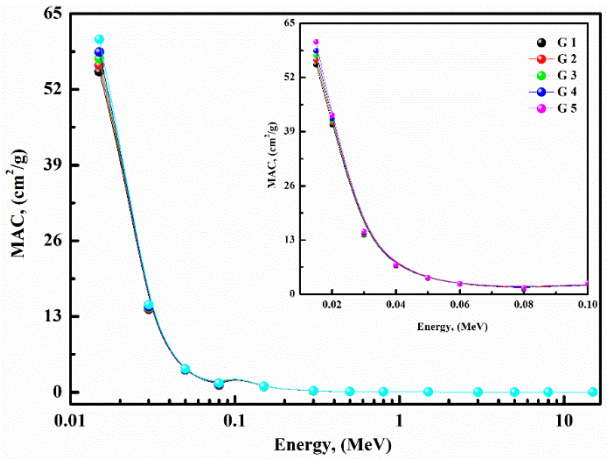

Fig. 13. MAC of prepared glasses.

The shielding properties of samples are frequently interpreted using one of the important armor parameters, HVL, TVL, and MFP. Figs 15, 16, & 17 show the results of these parameters for all of the glasses studied. Higher HVL, TVL, and MFP values indicate thicker glass used to attenuate gamma-ray photons. As a result, lower HVL, TVL, and MFP values indicate better shielding properties. The HVLS, TVLs & MFPs for photon energy decrease as the WO_3 concentration in glass increases. Furthermore, the HVL, TVL, and MFP are listed in the order G1, G2, G3, G4, and G5 in descending order.

3.5. Neutron shielding

Figure 18 demonstrates the effective removal of cross-section values $\sum R$ of the glass system. The $\sum R$ results take the range between 0.123 and 0.129 cm^{-1} as the WO_3 level rises. The highest $\sum R$ value is found in the G 5 sample with the highest WO_3 contribution (0.129 cm^{-1}).

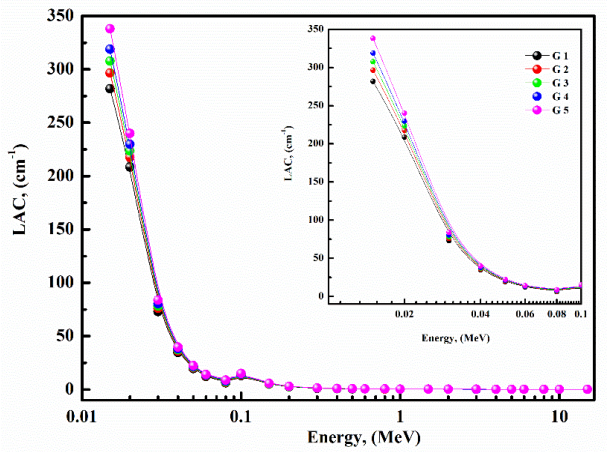

Fig. 14. LAC of prepared glasses.

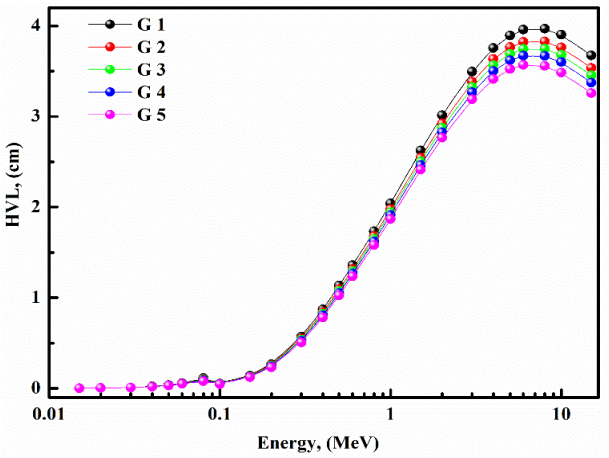

Fig. 15. HVL of prepared glasses.

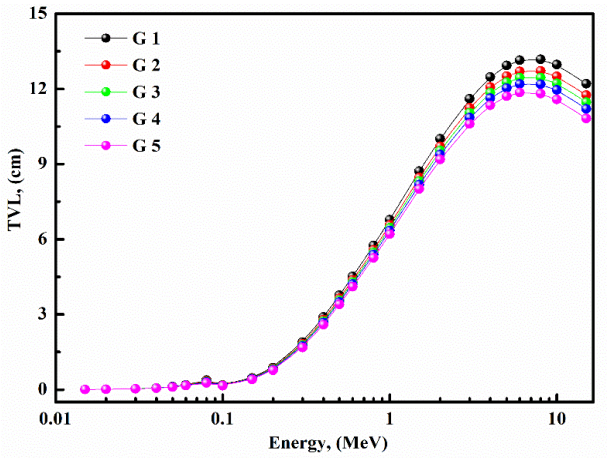

Fig. 16. TVL of prepared glasses.

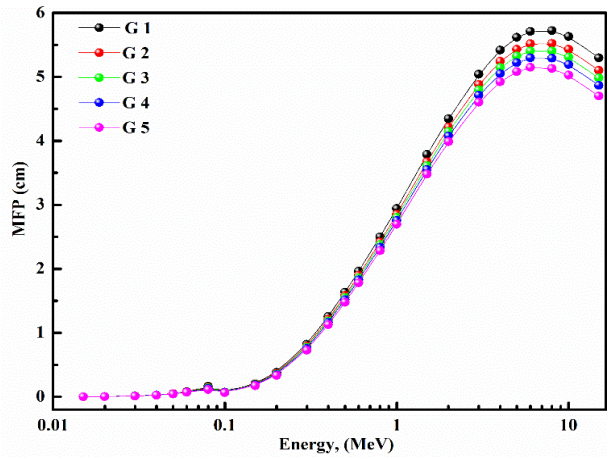

Fig. 17. MFP of prepared glasses.

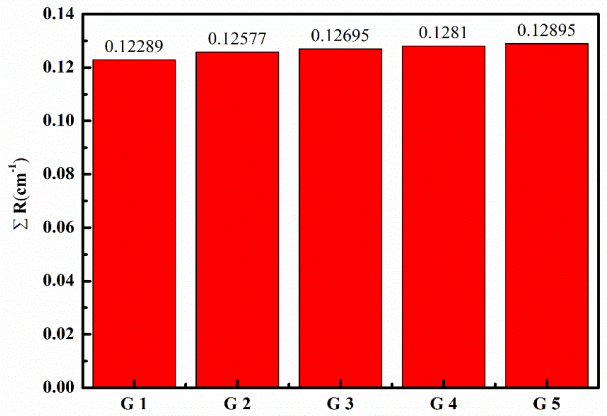

Fig. 18. FNRCS of prepared glasses.

4. Conclusion

The melt quenching technique was utilized to synthesize a set of arsenic lead phosphate glasses as formulation: $3As_2O_3 - 37PbO - (60 - x)\ P_2O_5$- $x\ WO_3$, x = ($0 \leq x \leq 5$ mol. %). The glasses' physical and other structural characteristics were examined in depth. The density, ultrasonic velocity, and elastic moduli of the glasses increased as the WO_3 content of the glasses increased. The results explore good agreement between the experimental and theoretical elastic moduli values by Makishima-Mackenzie model.

Due to P–O–W bonds in the glass network than P–O–P bonds, physical, structural, mechanical, and radiation properties were enhanced as the content of WO_3 increased. To understand the ability of radiation shielding for sample glasses that are doped with WO_3, important radiation shielding parameters such as MAC, LAC, TVL, HVL, MFP, and $\sum R$ are calculated. The results show that as the WO_3 content increases, the values of MAC, LAC, and $\sum R$ increase. According to this investigation, the G 5 sample can be used as shield from high photons energy and neutrons, and it is more effectively than the other fabricated arsenic lead phosphate glass.

Acknowledgments

Our gratitude to Princess Nourah bint Abdulrahman University Researchers Supporting Project number (PNURSP2023R326), Princess Nourah bint Abdulrahman University, Riyadh, Saudi Arabia.

References

[1] Temir, A., Zhumadilov, K., Zdorovets, M., Kozlovskiy, A., Trukhanov, A., 2021, Solid State Sciences 115, 106604; https://doi.org/10.1016/j.solidstatesciences.2021.106604

[2] Alomairy, S., Al-Buriahi, M.S., Abdel Wahab, E.A., Sriwunkum, C., Shaaban, K., 2021, Ceramics International 47, 17322-17330; https://doi.org/10.1016/j.ceramint.2021.03.045

[3] Alomairy, S., Alrowaili, Z.A., Kebaili, I., Wahab, E.A.A., Mutuwong, C., Al-Buriahi, M.S., Shaaban, K.S., 2021, Silicon; https://doi.org/10.1007/s12633-021-01347-2

[4] Wahab, E.A.A., Shaaban, K.S., Al-Baradi, A.M., 2021, Silicon; https://doi.org/10.1007/s12633-021-01236-8

[5] Mohan Babu, M., Syam Prasad, P., Hima Bindu, S., Prasad, A., Venkateswara Rao, P., Putenpurayil Govindan, N., Veeraiah, N., Özcan, M., 2020, Journal of Composites Science 4, 129; https://doi.org/10.3390/jcs4030129

[6] Shaaban, K.S., Zahran, H.Y., Yahia, I.S., Elsaeedy, H.I., Shaaban, E.R., Makhlouf, S.A., Wahab, E.A.A., Yousef, E.S., (2020), Applied Physics A 126; https://doi.org/10.1007/s00339-020-03982-9

[7] Sayed, M.A., Ali, A.M., Abd El-Rehim, A.F. et al. 2021, Journal of Elec Materi 50, 3116-3128; https://doi.org/10.1007/s11664-021-08921-9

[8] Shaaban, K.S., Yousef, E.S., Mahmoud, S.A., Wahab, E.A.A., Shaaban, E.R., (2020), Journal of Inorganic and Organometallic Polymers and Materials 30, 4655-4663; https://doi.org/10.1007/s10904-020-01574-x

[9] El-Taher, A., Ali, A.M., Saddeek, Y.B., Elsaman, R., Algarni, H., Shaaban, K., Amer, T.Z., (2019), Radiation Physics and Chemistry 165, 108403; https://doi.org/10.1016/j.radphyschem.2019.108403

[10] El-Maaref, A.A., Badr, S., Shaaban, K.S., Abdel Wahab, E.A., Elokr, M.M., (2019), Journal of Rare Earths 37, 253-259; https://doi.org/10.1016/j.jre.2018.06.006

[11] Abdel Wahab, E.A., El-Maaref, A.A., Shaaban, K.S., Börcsök, J., Abdelawwad, M., (2021), Optical Materials 111, 110638; https://doi.org/10.1016/j.optmat.2020.110638

[12] Gandhi, Y., Krishna Mohan, N., Veeraiah, N., 2011, Journal of Non-Crystalline Solids 357, 1193-1202; https://doi.org/10.1016/j.jnoncrysol.2010.11.016

[13] Srinivasarao, G., Veeraiah, N., 2002, Journal of Physics and Chemistry of Solids 63, 705-717; https://doi.org/10.1016/S0022-3697(01)00218-9

[14] Raghavaiah, B.V., Veeraiah, N., 2004, Journal of Physics and Chemistry of Solids 65, 1153-1164; https://doi.org/10.1016/j.jpcs.2004.01.004

[15] Shaaban, K.S., Saddeek, Y.B., (2017), Silicon 9, 785-793; https://doi.org/10.1007/s12633-017-9558-5

[16] El-Rehim, A.F.A., Shaaban, K.S., Zahran, H.Y., Yahia, I.S., Ali, A.M., Halaka, M.M.A., Makhlouf, S.A., Wahab, E.A.A., Shaaban, E.R., (2021), Journal of Inorganic and Organometallic Polymers and Materials 31, 1057-1065; https://doi.org/10.1007/s10904-020-01708-1

[17] Alothman, M.A., Alrowaili, Z.A., Alzahrani, J.S., Wahab, E.A.A., Olarinoye, I.O., Sriwunkum, C., Shaaban, K.S., Al-Buriahi, M.S., (2021), Journal of Alloys and Compounds 882, 160625; https://doi.org/10.1016/j.jallcom.2021.160625

[18] El-Rehim, A.F.A., Ali, A.M., Zahran, H.Y., Yahia, I.S., Shaaban, K.S., 2021, Journal of Inorganic and Organometallic Polymers and Materials 31, 1774-1786; https://doi.org/10.1007/s10904-020-01799-w

[19] Şakar E, Özpolat ÖF, Alım B, Sayyed MI, Kurudirek M (2020) Radiation Phys Chem 166:108496; https://doi.org/10.1016/j.radphyschem.2019.108496

[20] Mahmoud, K.H., Alsubaie, A.S., Wahab, E.A.A., Abdel-Rahim, F.M., Shaaban, K.S., (2021), Silicon; https://doi.org/10.1007/s12633-021-01125-0

[21] Shaaban, K.S., Yousef, E.S., 2020. Optik 203, 163976; https://doi.org/10.1016/j.ijleo.2019.163976

[22] Alomairy, S., Aboraia, A.M., Shaaban, E.R., Shaaban, K.S., (2021). Brazilian Journal of Physics 51, 1237-1248; https://doi.org/10.1007/s13538-021-00928-1

[23] Ali, A.M., Alrowaili, Z.A., Al-Baradi, A.M., Al-Buriahi, M.S., Wahab, E.A.A., Shaaban, K.S., (2021), Silicon; https://doi.org/10.1007/s12633-021-01440-6

[24] El-Maaref, A.A., Wahab, E.A.A., Shaaban, K.S., El-Agmy, R.M., (2021), Solid State Sciences 113, 106539; https://doi.org/10.1016/j.solidstatesciences.2021.106539

[25] Shaaban, K.S., Koubisy, M.S.I., Zahran, H.Y., Yahia, I.S., 2020 Journal of Inorganic and Organometallic Polymers and Materials 30, 4999-5008; https://doi.org/10.1007/s10904-020-01640-4

[26] El-Maaref, A.A., El-Agmy, R.M., Shaaban, K.S., Abdel Wahab, E.A., (2021), The European Physical Journal Plus 136; https://doi.org/10.1140/epjp/s13360-021-01798-x

[27] El-Maaref, A.A., Wahab, E.A.A., Shaaban, K.S., Abdelawwad, M., Koubisy, M.S.I., Börcsök, J., Yousef, E.S., (2020), Spectrochimica Acta Part A: Molecular and Biomolecular Spectroscopy

242, 118774; https://doi.org/10.1016/j.saa.2020.118774

[28] Shaaban, K.H.S., Saddeek, Y.B., Aly, K., (2018), Ceramics International 44, 3862-3867; https://doi.org/10.1016/j.ceramint.2017.11.175

[29] Saddeek, Y.B., Aly, K.A., Shaaban, K.S., Ali, A.M., Sayed, M.A., (2019), Silicon 11, 1253-1260; https://doi.org/10.1007/s12633-018-9912-2

[30] Shaaban, K.S., Alrowaili, Z.A., Al-Baradi, A.M., Ali, A.M., Wahab, E.A.A., Al-Buriahi, M.S., 2021, Silicon; https://doi.org/10.1007/s12633-021-01441-5

[31] El-Rehim, A.F.A., Shaaban, K.S., (2021), Journal of Materials Science: Materials in Electronics 32, 4651-4671; https://doi.org/10.1007/s10854-020-05204-7

[32] Shaaban, K.S., Ali, A.M., Saddeek, Y.B., Aly, K.A., Dahshan, A., Amin, S.A., (2019), Silicon 11, 1853-1861; https://doi.org/10.1007/s12633-018-0004-0

[33] El-Rehim, A.F.A., Zahran, H.Y., Yahia, I.S., Wahab, E.A.A., Shaaban, K.S., (2021), Journal of Materials Engineering and Performance 30, 1872-1884; https://doi.org/10.1007/s11665-021-05513-w

[34] Alomairy, S., Aboraia, A.M., Shaaban, E.R., Shaaban, K.S., 2021, Brazilian Journal of Physics 51, 1237-1248; https://doi.org/10.1007/s13538-021-00928-1

[35] Abdel Wahab, E.A., Shaaban, K.S., Yousef, E.S., (2020), Optical and Quantum Electronics 52; https://doi.org/10.1007/s11082-020-02575-3

[36] Saddeek, Y B; Aly, K A; Shaaban, Kh S; Ali, Atif Mossad; Sayed, M A 2018, Materials Research Express, 5(6), 065204; https://doi.org/10.1088/2053-1591/aac93f

[37] Makishima, A., Mackenzie, J.D., (1973), Journal of Non-Crystalline Solids 12, 35-45; https://doi.org/10.1016/0022-3093(73)90053-7

[38] Makishima, A., Mackenzie, J.D., (1975), Journal of Non-Crystalline Solids 17, 147-157; https://doi.org/10.1016/0022-3093(75)90047-2

[39] El-Rehim, A.F.A., Zahran, H.Y., Yahia, I.S., Ali, A.M., Shaaban, K.S., (2020), Silicon; https://doi.org/10.1007/s12633-020-00827-1

[40] El-Rehim, A.F.A., Zahran, H.Y., Yahia, I.S., Makhlouf, S.A., Shaaban, K.S., (2021), Silicon 13, 2289-2307; https://doi.org/10.1007/s12633-020-00798-3

[41] Shaaban, K.S., Alomairy, S., Al-Buriahi, M.S., (2021), Journal of Materials Science: Materials in Electronics; https://doi.org/10.1007/s10854-021-05885-8

[42] Shaaban, K.S., Boukhris, I., Kebaili, I., Al-Buriahi, M.S., (2021), Silicon; https://doi.org/10.1007/s12633-021-01080-w

[43] Al-Baradi, A.M., El-Rehim, A.F.A., Alrowaili, Z.A., Al-Buriahi, M.S., Shaaban, K.S., 2021, Silicon; https://doi.org/10.1007/s12633-021-01481-x

[44] Saddeek, Y.B., Shaaban, K.H.S., Elsaman, R., El-Taher, A., Amer, T.Z., (2018), Radiation Physics and Chemistry 150, 182-188; https://doi.org/10.1016/j.radphyschem.2018.04.028

[45] B. Albarzan, Aljawhara H. Almuqrin, M.S. Koubisy, E.A. Abdel Wahab, K.A. Mahmoud, Kh.S. Shaaban, M.I. Sayyed, (2021), Progress in Nuclear Energy,141,103931; https://doi.org/10.1016/j.pnucene.2021.103931

[46] Abdel Wahab, E.A., Shaaban, K.S., Alomairy, S., Al-Buriahi, M.S., (2021), The European Physical Journal Plus 136; https://doi.org/10.1140/epjp/s13360-021-01572-z

[47] Alrowaili, Z.A., Al-Baradi, A.M., Sayed, M.A., Mossad Ali, A., Abdel Wahab, E.A., Al-Buriahi, M.S., Shaaban, K.S., (2021), Optik 168259; https://doi.org/10.1016/j.ijleo.2021.168259

[48] Fayad, A.M., Shaaban, K.S., Abd-Allah, W.M., Ouis, M., (2020), Journal of Inorganic and Organometallic Polymers and Materials 30, 5042-5052; https://doi.org/10.1007/s10904-020-01641-3

[49] Kavaz, E., El_Agawany, F.I., Tekin, H.O., Perişanoğlu, U., Rammah, Y.S., 2020, Journal of Physics and Chemistry of Solids 142, 109437; https://doi.org/10.1016/j.jpcs.2020.109437

[50] Abouhaswa, A.S., Tekin, H.O., Kavaz, E., Perişanoğlu, U., 2021, Radiation Physics and Chemistry 183, 109428; https://doi.org/10.1016/j.radphyschem.2021.109428